SERS-Coded Gold Nanorods as a Multifunctional Platform for Densely Multiplexed Near-Infrared Imaging and Photothermal Heating

By *Geoffrey von Maltzahn, Andrea Centrone, Ji-Ho Park, Renuka Ramanathan, Michael J. Sailor, T. Alan Hatton,* and *Sangeeta N. Bhatia**

Multifunctional nanomaterials have the potential to integrate the clinical paradigms of imaging and therapy to enable real-time visualization of therapeutic biodistributions in patients. For cancer therapy, nanomaterials with capacities to be remotely detected and triggered for therapy could also close the loop between tumor detection and treatment. In this work, we show that the near-infrared plasmon resonance of gold nanorods (NRs) may be exploited to provide an integrated platform for multiplexed Raman detection and remote-controlled photothermal heating. By screening mixed-monolayer NRs, coated with polyethyleneglycol polymers alongside visible- and NIR-absorbing molecules, we achieved surface-enhanced, resonant Raman scattering (SERRS) and identified three NR formulations that may be uniquely distinguished over a spectral bandwidth of only 6 nm in the near-infrared, a spectral multiplexing density over an order of magnitude greater than attainable with semiconductor quantum dots,[1] organic fluorochromes, and Raleigh scattering nanoparticle imaging approaches.[2–5] Given the characteristic Raman fingerprint of the molecular labels on the NRs, we refer to them hereafter as SERS-coded NRs. SERS-coded NRs are found to be highly stable, to be detectable down to attomolar particle concentrations, and to have low baseline cytoxicity in vitro. In vivo, SERS-coded NRs were efficiently detected following subcutaneous or intratumoral injection and enabled remote photothermal tumor heating to ablative temperatures. In the future, the dense near-infrared spectral multiplexing of gold NRs should catalyze efficient, multivariable screening of NR surface chemistries in a single animal host, as well as provide a route towards characterizing multicomponent nanoparticle systems with cooperative in vivo functions.

Raman imaging of nanomaterials has recently emerged as an attractive alternative to fluorescence approaches.[6–10] Raman spectroscopy is a desirable modality for in vivo imaging because, as opposed to semiconductor quantum dot labels,[1] Raman scattering may be both efficiently excited and detected within the near-infrared optical window (~700–900 nm), where endogenous tissue absorption coefficients are over two orders of magnitude lower than for blue and ultra-violet light.[11] Raman detection is also considerably less sensitive to photobleaching than fluorescence[7,12] and the characteristic bandwidths of Raman lines are up to two orders of magnitude narrower than for fluorescence. To date, Raman scattering from nanomaterials has been utilized to improve diagnostic sensitivity in vitro,[10,13–15] to probe subcellular environments,[16,17] and, very recently, to track spherical gold nanoparticles[6,7] and carbon nanotubes[18] in vivo. These in vivo studies highlight the potential for Raman spectroscopy to serve as an ultra-sensitive medical imaging modality.

In addition to their applications in diagnosis and imaging, plasmonic materials have recently attracted attention for their potential to serve as targeted nanoantennas for selective tumor ablation. Ablative tumor therapies have had the longstanding potential to provide a robust method of cancer destruction, yet traditional means for delivering external energy into tumors lack selectivity over surrounding normal tissues, requiring complex implementation strategies, and resulting in morbidity due to off-target heating. Plasmonic nanoantennas offer an opportunity to alter this paradigm by extrinsically imparting their optical properties to tumor tissue and enabling deposition of otherwise benign near-infrared energy into tumors. Gold nanoshells, core–shell nanomaterials with tunable plasmon resonance, have shown considerable efficacy for these applications in mice.[19–21] More recently, gold NRs have emerged as attractive materials for these applications due to their small size, ability to be synthesized in bulk, narrow spectral bandwidth, and theoretical per micrometer

[*] Prof. S. N. Bhatia, G. von Maltzahn, R. Ramanathan
Harvard-MIT Division of Health Sciences and Technology
Massachusetts Institute of Technology
77 Massachusetts Avenue, Cambridge, MA 02139 (USA)
E-mail: sbhatia@mit.edu

Prof. S. N. Bhatia
Electrical Engineering and Computer Science, MIT
David H. Koch Institute for Integrative Cancer Research
Department of Medicine, Brigham and Women's Hospital,
and Howard Hughes Medical Institute
Boston, MA (USA)

Prof. T. A. Hatton, Dr. A. Centrone
Department of Chemical Engineering
Massachusetts Institute of Technology
77 Massachusetts Avenue, Cambridge, MA 02139 (USA)

Prof. M. J. Sailor, J.-H. Park
Materials Science and Engineering Program
Department of Chemistry and Biochemistry
University of California, San Diego
9500 Gilman, La Jolla, CA 92093 (USA)

Prof. M. J. Sailor
Departments of Bioengineering and Nanoengineering
University of California, San Diego
9500 Gilman, La Jolla, CA 92093 (USA)

DOI: 10.1002/adma.200803464

absorption coefficients over an order of magnitude higher than observed for gold nanoshells.[2,22–26] NRs have also been utilized for optical imaging, either via two-photon fluorescence or via Raleigh scattering.[4,5] Here, we provide the first molecular encoding of Raman signatures into NRs for integrated in vivo detection and remote-controlled photothermal heating (Fig. 1A and B).

Briefly, the synthesis of SERS-coded PEG-NRs involved the use of exhaustive dialysis to displace cetyltrimethylammonium bromide (CTAB) layers on the NR surface gradually and allow binding of thiolated polymers and Raman-active molecules (Fig. 1B).[6,27] In agreement with others,[28] we found CTAB-coated NRs to be highly stable, preventing thiol and reporter molecule adsorption to the NR surface even under high thiol-PEG concentrations. Further, sequential centrifugation of NRs to remove CTAB surfactant resulted in particle destabilization and agglomeration. By dialyzing mixtures of CTAB-NRs with reporter and thiol-PEG molecules against large baths (>100× volumetrically) of reporter molecules, we were able to drive CTAB displacement, while allowing PEG/reporter molecules access to the gold surface. Dialysis membranes were chosen so as to retain thiol-PEG polymers and NRs within the tubing, while allowing free transit of monomer CTAB molecules and reporter molecules.

Noble metal nanosized objects like spherical NPs and NRs have a characteristic plasmon frequency that depends on their size and shape[29–31] but unlike spherical NPs, NRs can be engineered to have the plasmon resonance[30,32] within the near-infrared optical window for in vivo applications. We utilized gold NRs with peak plasmon resonance at 790 nm, designed to match our near-infrared SERS excitation source (785 nm) and still provide strong optical absorption at 810 nm for photothermal heating (Fig. 2A). To begin, we screened a series of SERS active molecules widely used in the literature like crystal violet (**I**, CV), malachite green (**II**, MG), nile blue (**III**, NB) and some less common molecules like 3,3′-diethylthiatricarbocyanine iodide (**IV**, DTTC-765), aluminum 1,8,15,22-tetrakis(phenylthio)-29H,31H-phthalocyanine chloride (**V**, Al-TPPC), IR-792 perchlorate (**VI**, IR-792), with optical absorption in the NIR to achieve resonant SERS conditions on NRs (Fig. 1B). We also analyze molecules very similar to **IV**, like 3,3′-diethylthiadicarbocyanine iodide (**VII**, DTDC-655) and 3,3′-diethylthiacarbocyanine iodide (**VIII**, DTC-560) to evaluate the resonant Raman scattering intensity contribution (Fig. 1B). surface enhanced Raman scattering (SERS)[33–35] exploits the potential for noble metal surfaces to enhance the Raman scattering of adsorbed molecules up to 10^{14} fold. SERS was initially observed on roughened silver surfaces;[36,37] and recently it was shown that silver or gold NPs can provide single molecule detection.[38,39] The enhancement, up to 10^{14} times,[34] is attributed to two contributions, named chemical and electromagnetic effects. The electromagnetic effect arises when the metal plasmon resonance, a collective oscillation of conduction band electrons (Fig. 1A and 2A), is excited by the laser light leading to a strong enhancement of the local electromagnetic field and consequently to an intensification of the Raman effect up to 12 orders of magnitude.[40] The chemical effect is due to the formation of a charge transfer state between the metal and the adsorbed molecule and accounts for an enhancement of up to two orders of magnitude.[34] Resonant Raman scattering is achieved when the exciting laser light wavelength matches the optical absorption of the Raman active molecule; in this condition the Raman scattering can be further enhanced by two orders of magnitude.[40]

The best SERS-coded NRs were selected by comparing the ratio of the most intense SERS peak height of each dye to the peak

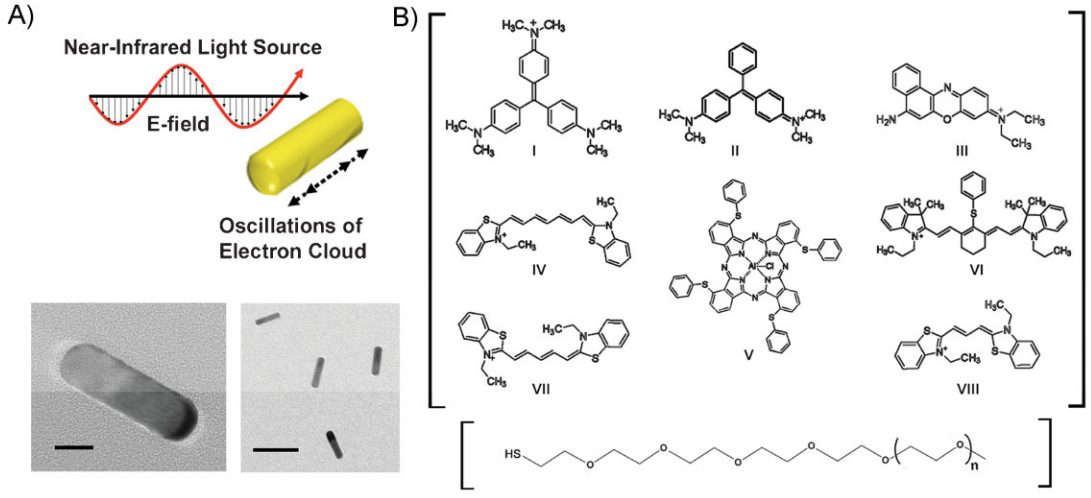

Figure 1. Structure of gold NRs, SERS-active molecules, and PEG polymer utilized in synthesis of SERS-coded PEG-NRs. A) Schematic and TEM images of gold NRs used in this study (scale bars = 10 and 60 nm for left and right images, respectively). In an applied near-infrared light source, the resonant oscillation of gold electrons is exploited to provide both enhanced remote detection via SERS from binary molecule/polymer monolayers and local photothermal heating via thermal dissipation of absorbed energy. B) SERS-active molecules screened in this study alongside polyethylene glycol polymers (below, 5 kDa molecular weight used here) on the surface of NRs: I) crystal violet, $\lambda_{max} = 590$ nm; II) malachite green, $\lambda_{max} = 620$ nm; III) nile blue, $\lambda_{max} = 553$ nm; IV) 3,3′-diethylthiatricarbocyanine iodide, $\lambda_{max} = 765$ nm; V) aluminum 1,8,15,22-tetrakis(phenylthio)-29*H*,31*H*-phthalocyanine chloride, $\lambda_{max} = 759$ nm; VI) IR-792 perchlorate, $\lambda_{max} = 792$ nm; VII) 3,3′-diethylthiadicarbocyanine iodide $\lambda_{max} = 655$ nm; VIII) 3,3′-diethylthiacarbocyanine iodide $\lambda_{max} = 560$ nm.

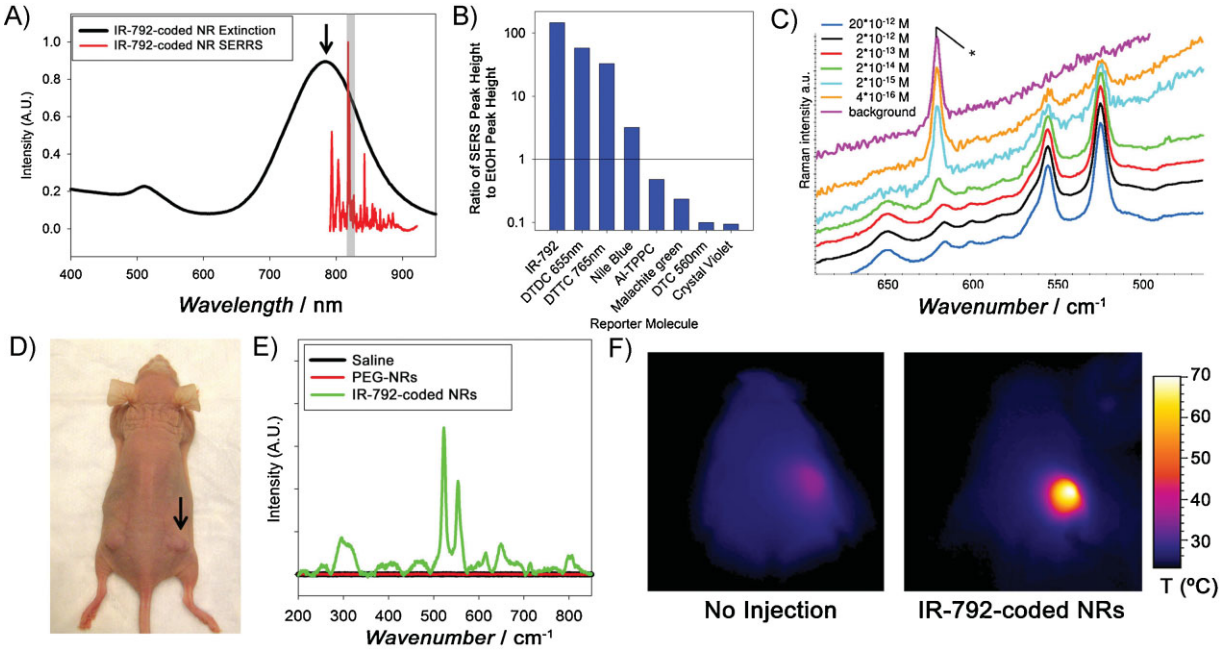

Figure 2. SERS-coded PEG-NRs for ultra-sensitive near-infrared detection and photothermal heating. A) Overlay of NIR absorption and emission of SERS-coded NRs. The arrow indicates the NIR Raman exciting-line and the gray column represents the wavelength of the diode laser source utilized for photothermal heating. B) Peak height ratios of the most intense SERS peak of each molecule with respect to the internal ethanol standard vibration at 879 cm^{-1}. C) SERS spectra of homogenous solutions of IR-792-coded NRs at various concentrations to explore the limit of detection. Spectra are displayed at full scale and offset for clarity to accommodate the intensity differences of several orders of magnitude. The relative intensity of the polystyrene multiwell plate line (*) increases with respect to the SERS spectra at low concentrations. D) Athymic (nu/nu) mice bearing bilateral human MDA-MB-435 tumors were injected intratumorally with either SERS-coded NRs, PEG-NRs, or saline (arrow) to evaluate potential for in vivo detection and photothermal heating. E) In vivo Raman spectra of IR-792-coded NRs, PEG-NRs and saline solution; 10 acquisitions of 4 s each were acquired for each spectrum. F) Infrared thermographic maps of mouse surface temperature 3 min after onset of irradiation with diode laser (810 nm, 2 W cm^2).

height of the ethanol vibration at 879 cm^{-1} used as an internal standard. Of the eight molecules tested, we identified the three near-infrared absorbing molecules IR-792 (**VI**), DTTC-765 (**IV**), and DTDC-655 (**VII**) to display a 10–10^3 fold higher signal than three molecules with visible absorbance shown previously to exhibit efficient near-infrared SERS on spherical gold nanoparticles (**I**, **II**, **III**)[6] (Fig. 2B). The characteristic scattering lines from these three molecules could be detected in homogenous solutions at attomolar or low femtomolar NR concentrations (Fig. 2C and S1 of the Supporting Information). By contrast, molecules tested alone (without NRs) showed no detectable Raman scattering even at millimolar concentrations. Several possible phenomena may underlie the differential Raman activity of molecule-coded NRs, including variable dye affinities or distributions on the NR surface, intrinsically different SERS cross-sections, or different contributions of the optical Raman resonance, or a combination of these. For the purpose of generating SERS-coded NRs that may be detected efficiently via Raman scattering, we conducted a screen to identify molecules that exhibited the largest SERS intensity for a given NR concentration. A few qualitative observations could be derived from these experiments that may be of guidance for future mechanistic work. The three thiacarbocyanine molecules (Fig. 1B: **IV**, **VII**, **VIII**) are characterized by very similar structures but with respectively decreasing electronic conjugation which should lead to smaller polarizability, Raman cross-section, and a decreasing resonant contribution for the shorter molecules, in accord with the experimental observation. On the other hand compounds **IV** and **V** have similar λ_{max} but very different SERS intensities per NR, suggesting different dye concentrations on the NR surfaces or different Raman cross-sections. Another effect that should be taken into account is that the SERS intensity is maximized when the wavelength of the plasmon peak is equally distant from the wavelength of the exciting laser and from the wavelength of the SERS active vibration.[41] However, this effect should have little influence for the three best coded-NRs because of the proximity of SERS active frequencies for these molecules.

We next investigated the capacity of SERS-coded NRs to provide both spectroscopic signatures and remote photothermal heating. To begin, the Raman spectra of three SERS-coded NRs were obtained and samples were subsequently irradiated with an 810 nm diode laser (2 W cm^2, 1.5 cm beam diameter) to evaluate their ability to be heated photothermally (Fig. S2). During irradiation, samples were imaged continuously using a thermographic infrared camera to monitor sample temperatures remotely. Irradiation at 810 nm rapidly heated all NR samples to 70 °C, while a saline control showed minimal temperature changes (Fig. S2), demonstrating the SERS-coded NRs retain their capacity to be heated photothermally. Further, we found that even following NR heating to ablative temperatures, the spectroscopic signatures of adsorbed molecules were retained (Fig. S3), indicating that molecule adhesion to the NR surface was not readily compromised and that SERS-coded NRs could be followed spectroscopically over the course of multiple

photothermal treatments. Using athymic (nu/nu) mice implanted with bilateral human MDA-MB-435 tumors (Fig. 2D), we injected 10 μL (20 fmol of NRs) of either SERS-coded PEG-NRs, PEG-NRs, or saline directly into the right flank tumor. After injection, Raman spectra of tumors were collected rapidly and enabled clear distinction of the three experimental groups, showing IR-792 NRs signatures with little background signal from PEG-NRs alone or from saline (Fig. 2E). Upon irradiation with an 810 nm diode laser (2 W cm^2), both NRs- and SERS-coded NRs-injected tumors rapidly heated to ablative temperatures above 75 °C, while saline-injected mice did not reach temperatures above ~40 °C (Fig. 2F and S4). This demonstration of remote detection and photothermal actuation highlights the potential for SERS-coded NRs to provide integrated imaging and therapy.

In addition to their efficient SERS detection under NIR excitation, we observed that the narrow Raman bandwidths (<1 nm FWHM) and spectral complexity of our best three SERS-coded NRs enabled them to be distinguished uniquely from one another within a very narrow spectral region of ~6 nm (816–822 nm; 500–600 cm^{-1}) (Fig. 3A). To evaluate whether SERS signatures could enable ultra-dense, quantitative spectral multiplexing of NRs solutions, a series of tertiary NR mixtures were created and detected to deduce relative species abundance spectrally (Fig. 3B). Across an order of magnitude of relative concentration variation, we found that spectral analysis readily predicted tertiary mixture compositions within a few percent error at picomolar total particle concentrations. To confirm that SERS-coded NRs could be distinguished spectrally in vivo following subcutaneous injection, tumor-free athymic mice were dorsally injected with 2 fmol of each the three SERS-coded NRs in discreet subcutaneous regions. Following injection, the Raman spectra of these regions and an uninjected control region were collected under 785 nm excitation. We found that the spectra of the three different SERS-coded NRs were readily distinguished in vivo with minimal background interference with spectral analysis of narrow SERS lines (Fig. 3C), highlighting the ability for multiple SERS signatures to be detected in vivo.

Finally, we studied the in vitro cytotoxicity of these materials to investigate whether the molecules conferring distinct Raman signatures to NRs affected the baseline cytotoxicity of their gold substrata. Gold nanoparticles and gold salts have been approved for clinical use in Rheumatoid arthritis therapies for decades and serve as relatively benign nanomaterial substrates for biological applications.[42,43] To assess the cytotoxicity of SERS-NRs, we

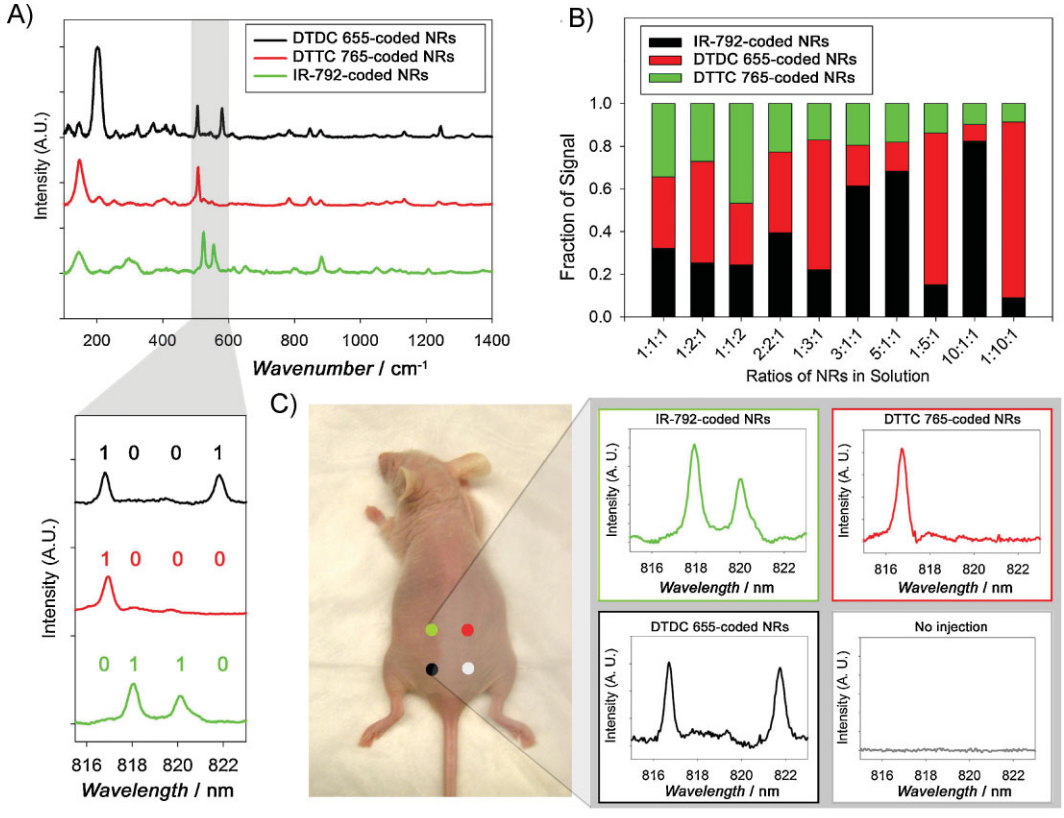

Figure 3. Ultradense near-infrared multiplexing of SERS-coded gold NRs in vitro and in vivo. A) In vitro SERS spectra of DTDC 655- (black), DTDC 765- (red), and IR-792-coded gold NRs after baseline correction. In gray, a 6 nm spectral region is highlighted to distinguish the three NR populations. B) Quantitative in vitro spectral multiplexing of tertiary SERS-coded NR solutions. Tertiary solutions of NRs (labeled on abscissa) were imaged and analyzed spectrally to predict mixture composition (bars indicate predicted abundance of each component). C) In vivo distinction of three SERS-coded NR populations. Athymic (nu/nu) mice were subcutaneously injected with each SERS-coded NR population in distinct locations and Raman spectra were recorded and compared to a region of naïve tissue.

utilized human HeLa cervical cancer cultures and assessed viability after 24 h of incubation with particles using the fluorogenic intracellular esterase sensor Calcein acetoxymethylester (Calcein AM). All three SERS-NRs displayed comparable cytotoxicity levels to PEG-NRs with each showing >70% cell viability at the highest NR concentrations tested (2 mM Au), a dose $>10^6$ times higher than the detection limit for PEG-NRs (Fig. S5). This provides encouraging evidence that molecule addition to PEGylated NR substrata can act as a benign means of encoding their identity.

In summary, we present the synthesis of molecule-coded gold NRs as a platform for multiplexed NIR detection, via an intense SERS effect, and remote-controlled therapy, via photothermal heating. We find that by coating NRs during dialysis, SERS-active molecules can be stably adsorbed within a protective PEG shell to confer intense Raman signatures to their substrates that are detectable down to attomolar NRs concentrations. We establish the potential for SERS-coded NRs to provide photothermal heating of tumors to ablative temperatures in vivo. Finally, we highlight the immense in vivo multiplexing potential for SERS-coded NRs. In addition to their therapeutic applications, the utility of nanomaterials for studying in vivo biology has expanded considerably and could benefit from methods for non-invasively testing multiple biological hypotheses. Over the past decade, semiconductor quantum dots have enabled a multitude of biological applications with their narrow (~30 nm FWHM), size-tunable fluorescent emission and ability for multiple particles to be excited using a single UV source.[1] Here, we show that under a NIR excitation source, three unique Raman-coded NRs may be distinguished efficiently within ~6 nm of spectral bandwidth, while leaving a considerable portion of the NIR for future molecule-coded NR multiplexing. Moving forward, we envision that broader screening for efficient molecule-coded NRs and multivariate spectral analysis could enable the simultaneous imaging of >10 spectrally unique SERS-coded NRs under a single NIR excitation source, providing a novel route towards highly parallel in vivo screening of nanoparticle behavior.

Experimental

CTAB-coated gold NRs were purchased from Nanopartz with a peak plasmon resonance at 790 nm. To replace CTAB-monolayers, solutions of CTAB-NRs were brought to between 1 and 5 μM of one of eight reporter molecules and 100 μM of 5 kDa thiol-PEG and dialyzed for 24–48 h in a 5 kDa cutoff cellulose ester membrane (SpectraPor). After dialysis, NRs were purified further with multiple rounds of centrifugation using molecular weight cutoff centrifugal filters (100 kDa cutoff, Millipore) and stored at 200 pM at 4 °C.

A Horiba Jobin Yvon Labram HR800 spectrometer was used for recording the SERS spectra. Spectra were acquired with a 785 nm diode laser using a 600 grooves mm^{-1} grating and a 10× long working distance microscope objective. Under these conditions, the spectral resolution in the multiplexing region between 500 and 590 cm^{-1} was 4 cm^{-1} (or 0.3 nm between 817 and 823 nm). In vitro spectra were acquired between 100 and 1900 cm^{-1} of Raman shift using 50 mW of laser power.

The SERS intensities of NRs coated with different dyes were compared using ethanol as an internal standard; namely ethanol (500 μL) was mixed with a NR water solution (1500 μL) in a 2 mL closed glass vial. The best NRs were selected by comparing the peak height ratio of the dye's most intense SERS peak to the peak height of the ethanol vibration at 879 cm^{-1} used as an internal standard. The comparison was made with NRs from the same batch coated with different dyes under identical conditions. The error due to the baseline choice on the peak ratio was minimal when the two peaks had approximately the same height; because of that the initial 200 pM NR solutions were diluted up to 15 times for the NRs with the strongest SERS intensity and the dilution factor was taken into account in the comparison. The limit of detection for the three best SERS-active NRs was determined using 60-second acquisitions, analyzing solutions at various concentrations from 20×10^{-12} M (1 o.d.) up to 4×10^{-16} M.

Photothermal experiments were conducted under the guidance of infrared thermography (FLIR S60 camera). A custom 30 W, variable output 810 nm diode laser source was utilized for thermographic experiments. All in vitro and in vivo experiments were conducted using a 1.5 cm diameter and 2 W cm^2 intensity beam. For in vitro experiments, tubes of NRs at 200 pM were irradiated for 5 min to reach 70 °C and cooled to room temperature. Samples from before and after irradiation were saved for Raman imaging to analyze whether photothermal heating compromised spectral signatures. For photothermal tumor heating experiments, human MDA-MB-435 cancer cells (ATTC) were cultured as recommended and injected bilaterally in the flank of athymic (nu/nu) mice (~2E6 cells/tumor). At 2 weeks following implantation, tumors of ~300 mm^3 had formed and mice were selected for intratumoral injection of coded-NRs or control NRs. Mice were anaesthetized using either gas isofluorane or Ketaset/Midazalam liquid anesthetic and 10 μL of a 2 nM solution of NRs were injected intratumorally for subsequent Raman spectroscopy and photothermal experiments. For in vivo multiplexing, tumor-free athymic (nu/nu) mice were anaesthetized and injected subcutaneously with 10 μL of a 200 pM NR solution for imaging.

Cytotoxicity assessments were conducted using Human HeLa cervical cancer cultures (ATTC) in 96 well plates grown to ~70% confluency. Cells were incubated with one of three SERS-coded gold NR formulations or unlabeled PEG-NRs and assessed for viability after 24 h of incubation using the fluorogenic intracellular esterase sensor Calcein acetoxymethylester (Calcein AM, Invitrogen).

All animal experiments were conducted under the guidelines of the MIT Committee for Animal Care.

Acknowledgements

G. M. and A. C. contributed equally to this work. This project was funded in part with Federal funds from the National Cancer Institute of the National Institutes of Health (Contract No. N01-C0-37117, R01CA124427-01, UO1 HL 080718). M. J. S. and S. N. B. are members of the Moores UCSD Cancer Center and the UCSD NanoTUMOR Center under which this research was conducted and partially supported by NIH Grant U54 CA 119335. G. M. acknowledges generous funding by NSF and Whitaker Graduate Fellowships. We thank Dr. Yoel Fink for generous use of the infrared camera used in this work and Dr. A. Garratt-Reed for assistance with TEM imaging. We gratefully acknowledge Dr. C. Schoen and Dr. S. Coldiron for developing the CTAB-coated parent formulations utilized in this work. Supporting Information is available online from Wiley InterScience or from the author.

Received: November 25, 2008
Revised: February 20, 2009
Published online: April 20, 2009

[1] X. Michalet, F. F. Pinaud, L. A. Bentolila, J. M. Tsay, S. Doose, J. J. Li, G. Sundaresan, A. M. Wu, S. S. Gambhir, S. Weiss, *Science* **2005**, *307*, 538.
[2] C. J. Murphy, T. K. San, A. M. Gole, C. J. Orendorff, J. X. Gao, L. Gou, S. E. Hunyadi, T. Li, *J. Phys. Chem. B* **2005**, *109*, 13857.
[3] S. Link, M. A. El-Sayed, *Int. Rev. Phys. Chem.* **2000**, *19*, 409.
[4] C. Yu, H. Nakshatri, J. Irudayaraj, *Nano Lett.* **2007**, *7*, 2300.
[5] H. Wang, T. B. Huff, D. A. Zweifel, W. He, P. S. Low, A. Wei, J. X. Cheng, *Proc. Natl. Acad. Sci. USA* **2005**, *102*, 15752.

[6] X. M. Qian, X. H. Peng, D. O. Ansari, Q. Yin-Goen, G. Z. Chen, D. M. Shin, L. Yang, A. N. Young, M. D. Wang, S. M. Nie, *Nat. Biotechnol.* **2008**, *26*, 83.

[7] S. Keren, C. Zavaleta, Z. Cheng, A. de la Zerda, O. Gheysens, S. S. Gambhir, *Proc. Natl. Acad. Sci. USA* **2008**, *105*, 5844.

[8] Z. Chen, S. M. Tabakman, A. P. Goodwin, M. G. Kattah, D. Daranciang, X. Wang, G. Zhang, X. Li, Z. Liu, P. J. Utz, K. Jiang, S. Fan, H. Dai, *Nat. Biotechnol.* **2008**, *26*, 1285.

[9] Z. Liu, X. Li, S. M. Tabakman, K. Jiang, S. Fan, H. Dai, *J. Am. Chem. Soc.* **2008**, *130*, 13540.

[10] D. S. Grubisha, R. J. Lipert, H. Y. Park, J. Driskell, M. D. Porter, *Anal. Chem.* **2003**, *75*, 5936.

[11] R. Weissleder, *Nat. Biotechnol.* **2001**, *19*, 316.

[12] M. D. Porter, R. J. Lipert, L. M. Siperko, G. Wang, R. Narayanana, *Chem. Soc. Rev.* **2008**, *37*, 1001.

[13] Y. W. C. Cao, R. C. Jin, C. A. Mirkin, *Science* **2002**, *297*, 1536.

[14] M. J. Banholzer, J. E. Millstone, L. D. Qin, C. A. Mirkin, *Chem. Soc. Rev.* **2008**, *37*, 885.

[15] R. C. Jin, Y. C. Cao, C. S. Thaxton, C. A. Mirkin, *Small* **2006**, *2*, 375.

[16] J. Kneipp, H. Kneipp, M. McLaughlin, D. Brown, K. Kneipp, *Nano Lett.* **2006**, *6*, 2225.

[17] C. E. Talley, L. Jusinski, C. W. Hollars, S. M. Lane, T. Huser, *Anal. Chem.* **2004**, *76*, 7064.

[18] C. Zavaleta, A. de la Zerda, Z. Liu, S. Keren, Z. Cheng, M. Schipper, X. Chen, H. Dai, S. S. Gambhir, *Nano Lett.* **2008**, *8*, 2800.

[19] L. R. Hirsch, R. J. Stafford, J. A. Bankson, S. R. Sershen, B. Rivera, R. E. Price, J. D. Hazle, N. J. Halas, J. L. West, *Proc. Natl. Acad. Sci. USA* **2003**, *100*, 13549.

[20] D. P. O'Neal, L. R. Hirsch, N. J. Halas, J. D. Payne, J. L. West, *Cancer Lett.* **2004**, *209*, 171.

[21] A. M. Gobin, M. H. Lee, N. J. Halas, W. D. James, R. A. Drezek, J. L. West, *Nano Lett.* **2007**, *7*, 1929.

[22] P. K. Jain, K. S. Lee, I. H. El-Sayed, M. A. El-Sayed, *J. Phys. Chem. B* **2006**, *110*, 7238.

[23] M. Hu, J. Y. Chen, Z. Y. Li, L. Au, G. V. Hartland, X. D. Li, M. Marquez, Y. N. Xia, *Chem. Soc. Rev.* **2006**, *35*, 1084.

[24] X. Huang, I. H. El-Sayed, W. Qian, M. A. El-Sayed, *J. Am. Chem. Soc.* **2006**, *128*, 2115.

[25] R. S. Norman, J. W. Stone, A. Gole, C. J. Murphy, T. L. Sabo-Attwood, *Nano Lett.* **2008**, *8*, 302.

[26] A. G. Skirtach, P. Karageorgiev, B. G. De Geest, N. Pazos-Perez, D. Braun, G. B. Sukhorukov, *Adv. Mater.* **2008**, *20*, 506.

[27] T. Niidome, M. Yamagata, Y. Okamoto, Y. Akiyama, H. Takahashi, T. Kawano, Y. Katayama, Y. Niidome, *J. Controlled Release* **2006**, *114*, 343.

[28] B. P. Khanal, E. R. Zubarev, *Angew. Chem. Int. Ed.* **2007**, *46*, 2195.

[29] J. N. Anker, W. P. Hall, O. Lyandres, N. C. Shah, J. Zhao, R. P. Van Duyne, *Nat. Mater.* **2008**, *7*, 442.

[30] M. A. El-Sayed, *Acc. Chem. Res.* **2001**, *34*, 257.

[31] A. Centrone, E. Penzo, M. Sharma, J. W. Myerson, A. M. Jackson, N. Marzari, F. Stellacci, *Proc. Natl. Acad. Sci. USA* **2008**, *105*, 9886.

[32] C. J. Orendorff, L. Gearheart, N. R. Jana, C. J. Murphy, *Phys. Chem. Chem. Phys.* **2006**, *8*, 165.

[33] R. L. Garrell, *Anal. Chem.* **1989**, *61*, A401.

[34] K. Kneipp, H. Kneipp, I. Itzkan, R. R. Dasari, M. S. Feld, *Chem. Rev.* **1999**, *99*, 2957.

[35] G. C. Schatz, R. P. Vanduyne, *Surf. Sci.* **1980**, *101*, 425.

[36] M. Fleischm, P. J. Hendra, A. J. McQuilla, *Chem. Phys. Lett.* **1974**, *26*, 163.

[37] D. L. Jeanmaire, R. P. Vanduyne, *J. Electroanal. Chem.* **1977**, *84*, 1.

[38] W. E. Doering, S. M. Nie, *J. Phys. Chem. B* **2002**, *106*, 311.

[39] K. Kneipp, H. Kneipp, *Appl. Spectrosc.* **2006**, *60*, 322A.

[40] S. M. Nie, S. R. Emery, *Science* **1997**, *275*, 1102.

[41] A. D. McFarland, M. A. Young, J. A. Dieringer, R. P. Van Duyne, *J. Phys. Chem. B* **2005**, *109*, 11279.

[42] T. Pincus, G. Ferraccioli, T. Sokka, A. Larsen, R. Rau, I. Kushner, F. Wolfe, *Rheumatology* **2002**, *41*, 1346.

[43] J. N. Swanson, *Ann. Rheum. Dis.* **1949**, *8*, 232.

Submitted to ADVANCED MATERIALS

Supporting Information

SERS-Coded Gold Nanorods as a Multifunctional Platform for Densely-Multiplexed Near-Infrared Imaging and Photothermal Heating

By *Geoffrey von Maltzahn, Andrea Centrone, Ji-Ho Park, Renuka Ramanathan, Michael J. Sailor, T. Alan Hatton, Sangeeta N. Bhatia*

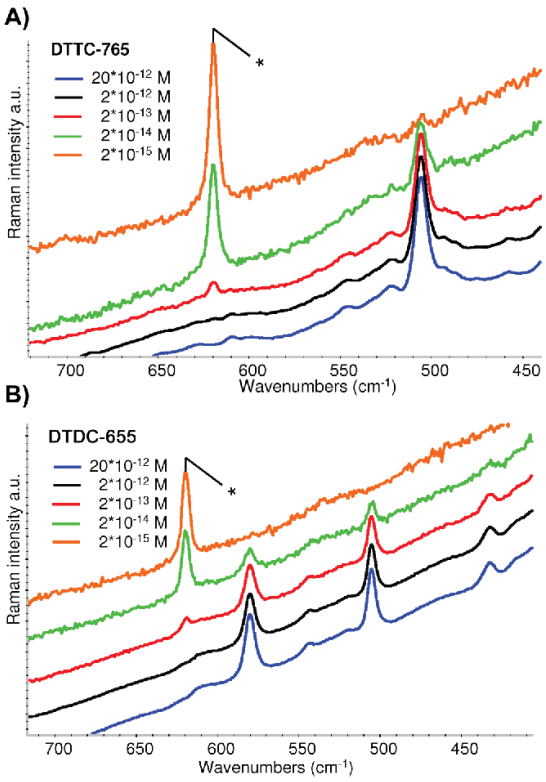

Figure 1S: Limit of detection of DTTC-765- and DTDC-655-coded nanorods. SERS spectra of DTTC-765-coded (A) and DTDC-655-coded NRs (B) at different concentrations show the limit of detection. Because of the many orders of magnitude in intensity difference, the spectra are displayed at full scale with an offset for clarity; at smaller concentrations the signal to noise ratio decreases and the relative intensity of the polystyrene line (*) of the multiwell plate increases with respect to the SERS spectra.

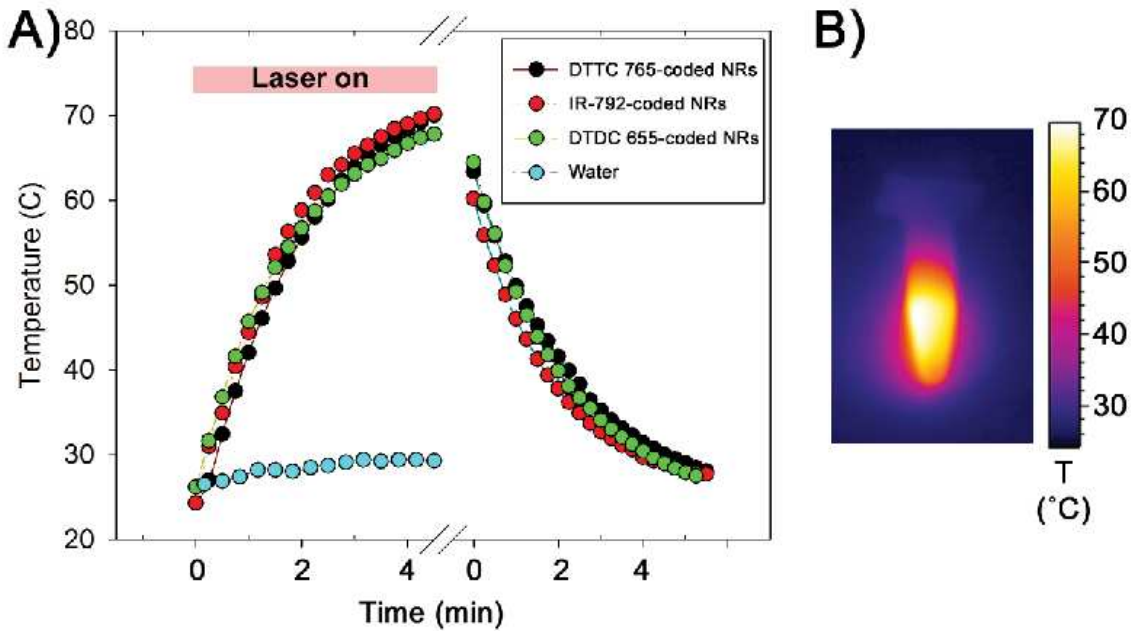

Figure 2S. Photothermal heating of SERS-coded nanorods *in vitro.* A) Samples of three SERS-coded nanorods and a saline control were irradiated with an 810nm diode laser ($2W/cm^2$, 1.5 cm beam diameter) for ~4 minutes while under continuous infrared surveillance with a thermographic camera to monitor sample temperatures. After heating of nanorod samples to 70˚C, laser irradiation was ceased and sample cooling was again monitored thermographically. B) A thermographic heat map of DTTC-765-coded nanorods at 4.5 minutes post onset of irradiation.

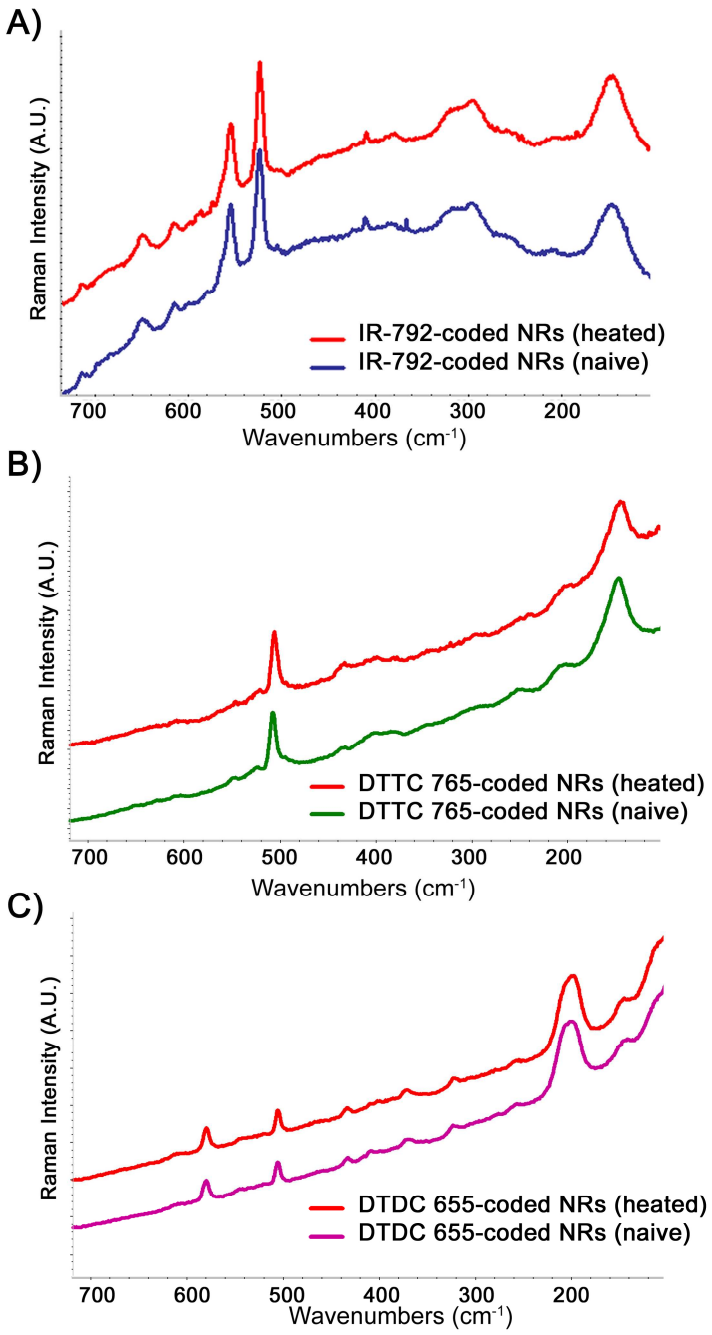

Figure 3S: Maintenance of SERS activity following photothermal heating. SERS spectra of IR 792-, DTTC-765-, and DTDC-655-coded NRs (A-C, respectively) before and after photothermal heating to 70°C. The spectra are displayed with an offset for clarity.

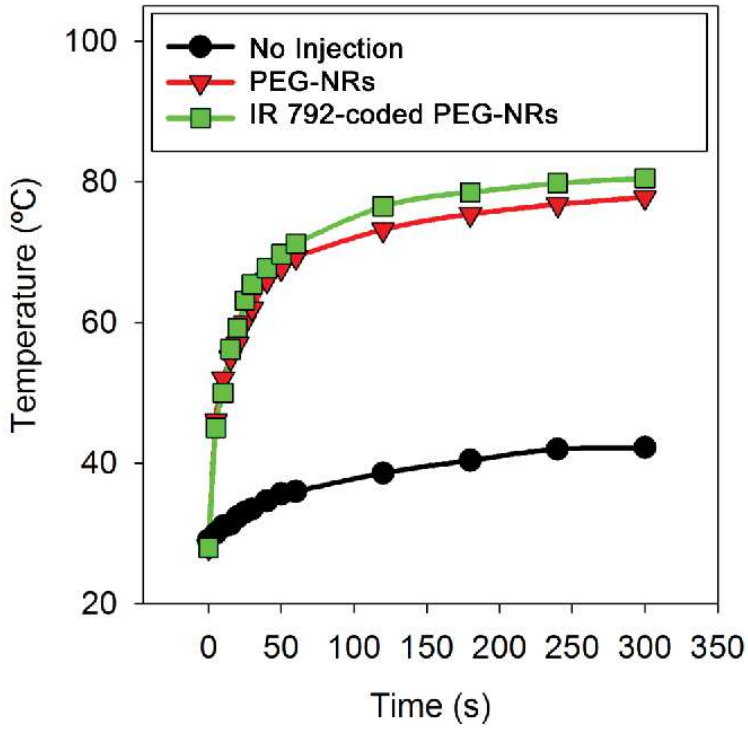

Figure 4S. **Photothermal heating of xenograft tumors *in vivo* following intratumoral injection.** Athymic (nu/nu) mice were intratumorally injected with SERS-coded- or unlabeled PEG-nanorods (20 femtomoles each) and irradiated with an 810nm diode laser source (2W/cm^2, 5 min) while under anesthesia. Infrared thermography was utilized to track maximum tumor temperatures over time following the onset of irradiation with comparison to a control tumor lacking nanorod antennas.

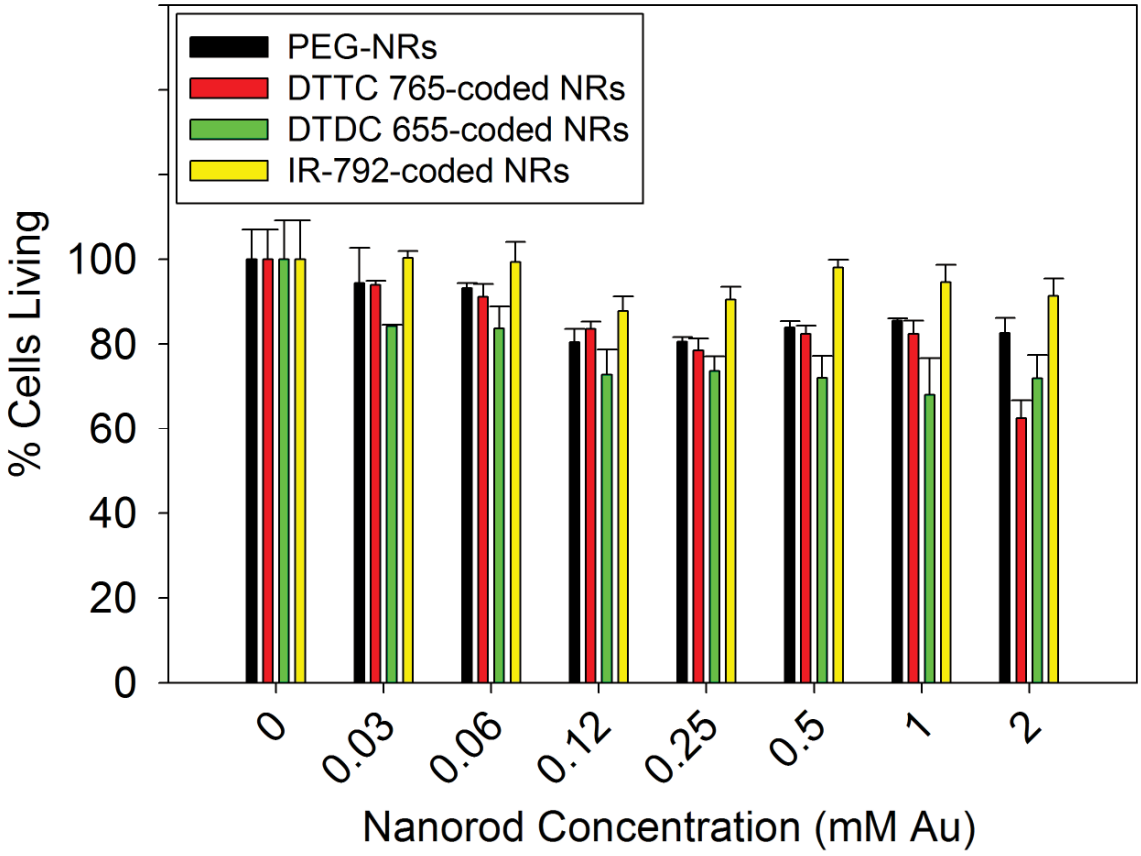

Figure 5S. Probing the cytotoxicity of SERS-coded gold nanorods compared to unlabeled gold nanorods. Human HeLa cervical cancer cultures were incubated with three SERS-coded gold nanorod formulations or unlabeled PEG-nanorods and viability after 24hrs of incubation with particles was assessed using the fluorogenic intracellular esterase sensor Calcein acetoxymethylester (Calcein AM).